Inorganic Chemistry

Forum Article

pubs.acs.org/IC

Metal–Organic Frameworks as Sensory Materials and Imaging Agents

Demin Liu, Kuangda Lu, Christopher Poon, and Wenbin Lin*

Department of Chemistry, University of Chicago, 929 E. 57th Street, Chicago, Illinois 60637, United States

ABSTRACT: Metal–organic frameworks (MOFs) are a class of hybrid materials self-assembled from organic bridging ligands and metal ion/cluster connecting points. The combination of a variety of organic linkers, metal ions/clusters, and structural motifs can lead to an infinite array of new materials with interesting properties for many applications. In this Forum Article, we discuss the design and applications of MOFs in chemical sensing and biological imaging. The first half of this article focuses on the development of MOFs as chemical sensors by highlighting how unique attributes of MOFs can be utilized to enhance sensitivity and selectivity. We also discuss some of the issues that need to be addressed in order to develop practically useful MOF sensors. The second half of this article focuses on the design and applications of nanoscale MOFs (NMOFs) as imaging contrast agents. NMOFs possess several interesting attributes, such as high cargo loading capacity, ease of postmodification, tunable size and shape, and intrinsic biodegradability, to make them excellent candidates as imaging contrast agents. We discuss the use of representative NMOFs in magnetic resonance imaging (MRI), X-ray computed tomography (CT), and optical imaging. Although still in their infancy, we believe that the compositional tunability and mild synthetic conditions of NMOF imaging agents should greatly facilitate their further development for clinical translation.

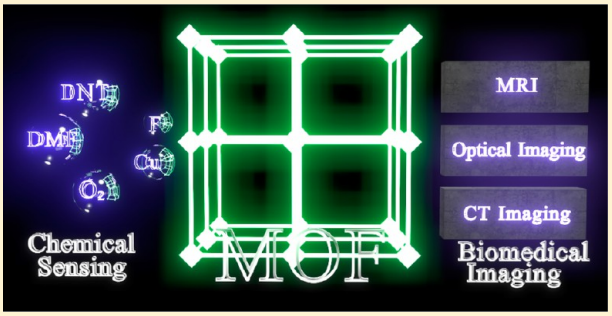

INTRODUCTION

Metal–organic frameworks (MOFs), also called porous coordination polymers, are an emerging class of crystalline porous materials composed of inorganic metal ions or clusters connected by polydentate organic linker ligands. Unlike traditional zeolites, which are comprised of SiO_4 and AlO_4 building blocks, the organic linkers in MOFs can be readily varied to allow for direct manipulation of their physical and chemical properties. Furthermore, MOFs are typically synthesized under mild conditions so a large variety of molecular functionalities can be rationally designed and incorporated into MOFs to impart desired properties for potential applications. Over the past 15 years, a large number of MOFs have been tailor-made for applications in many areas, including catalysis,[1−5] gas separation and storage,[6−9] nonlinear optics,[10] light harvesting,[11] and drug delivery.[12−14] MOFs have also recently been explored as sensory materials and imagining agents.

Chemical sensors have long been used in many applications, such as industrial hygiene,[15,16] quality control,[16,17] emission monitoring,[18−20] and clinical diagnostics.[21,22] Ideal chemical sensors should be highly sensitive to analytes of interest and yet remain unperturbed by other molecules or materials that may be present. In addition, the sensors must be stable so they can be stored for a long period of time and can be reused many times to reduce costs. The most investigated and commercially produced chemical sensors are inorganic[23,24] or organic semiconductor films[25,26] with typically ill-defined structures. Despite their versatile utility and commercial success, existing classes of chemical sensors can have limited sensitivity and selectivity. The crystalline and porous nature of MOFs endows them unique properties and offers several potential advantages over existing materials in chemical sensing. First, highly porous structures of MOFs can allow enhanced uptake of molecules or ions into their pores because of preferential interactions between molecules or ions and the pore surfaces. Such a preconcentration effect can enhance the sensitivity of the sensing moieties in MOFs. Second, the well-defined pore and channel structures of MOFs can exclude certain species to provide an additional mechanism for selective sensing that might not be operative in existing sensory materials. Third, the reduced conformational flexibility of sensing moieties in the frameworks of MOFs can also contribute to enhanced selectivity in molecular sensing. The first half of this Forum Article summarizes recent studies of MOFs as chemical sensors. We attempt to illustrate unique attributes of MOF sensors using literature examples and to highlight the potential advantages of MOFs over existing materials in chemical sensing.

When scaled down to the nanoregime, many of the bulk sensory materials can also be used as imaging agents for various diseases. Nanoparticles, in particular those of 20–200 nm in diameter, have several advantages over small-molecule imaging

Special Issue: Imaging and Sensing

Received: August 27, 2013
Published: November 19, 2013

   dx.doi.org/10.1021/ic402194c | *Inorg. Chem.* 2014, 53, 1916–1924

agents, such as high payloads, tunable sizes, tailorable surface properties, and improved pharmacokinetics.[27−30] Nanoparticles tend to have increased tumor uptake because of the enhanced permeability and retention (EPR) effect stemming from leaky neovasculatures and ineffective lymphatic drainage that are characteristic of tumors.[31] The accumulation of nanoparticles in tumors can be further enhanced by surface conjugation of cancer-specific ligands.[32,33] The Lin group first recognized the potential of nanoscale MOFs (NMOFs) as contrast agents for biomedical imaging. Prior to NMOFs, nanoparticle imaging agents are either purely inorganic or organic. It was hypothesized that NMOFs can combine attractive features of both inorganic and organic nanomaterials, such as chemical diversity, high loading capacity, and intrinsic biodegradability, to offer an entirely new class of imaging contrast agents. In the past few years, NMOFs have been explored as potential contrast agents for a number of imaging modalities, including magnetic resonance imaging (MRI), X-ray computed tomography (CT) imaging, and optical imaging (OI). The second half of this Forum Article discusses the potential use of NMOFs in biomedical imaging. We try to highlight recent literature on the design of NMOFs for various imaging applications.

■ MOFS AS SENSORS AND SENSORY MATERIALS

A chemical sensor must have desired selectivity, sensitivity, response times, material stability, and reusability. MOFs exhibit unique characteristics to become excellent chemical sensors. The porous nature of MOFs can potentially preconcentrate the analytes to achieve enhanced sensitivity. Meanwhile, the pores and channels can provide an ideal environment to accommodate the analyte molecules and to induce specific recognition. In the examples provided below, the selectivity of MOF sensors is derived from (1) channel size exclusion, (2) specific coordination or hydrogen bonding of analytes to the framework, (3) analyte-specific signal response, (4) host−guest chemistry in the MOF cavity, and (5) the chirality of the framework. In addition, amplified quenching was recently demonstrated with phosphorescent MOFs,[34] which provides an additional mechanism to significantly enhance the sensitivity of MOF sensors. Although MOF materials display outstanding stimulus response (sensing) properties, few of them have been used to construct sensing devices to date. Processing MOF materials into thin films[35] or nanocrystals[36,37] remains a hurdle for converting sensory MOF materials into functional sensing devices.

Size-Dependent Sensing of Gas Molecules. Lu and Hupp reported a ZIF-8 vapor sensor that displays chemical selectivity resulting from the small portal size of the cavities.[35] The ZIF-8 sensor was obtained in a thin-film form of controllable thickness (Figure 1a) by immersing glass or silicon slides in a freshly prepared methanolic solution of 2-methylimidazole and $Zn(NO_3)_2$ at room temperature. The sensing is based on Fabry-Pérot interference, which occurs when incident light reflects off two parallel surfaces separated by a distance, l, on the order of the wavelength of light. The wavelengths of the interference peaks can be determined by the following formula:

$$m\lambda = 2nl \quad (1)$$

where m is an integer and n is the thin film's refractive index.

When polarizable molecules enter the cavity, the overall reflective index will increase, resulting in red shifts of the interference peaks. The shift can be determined quantitatively as manifested by a propane/N_2 flow test at different propane partial pressures (Figure 1b,d). Although the response is not molecule-specific, the MOF sensor does display some chemical selectivity based on its channel size and the hydrophobic nature of the framework. For example, linear *n*-hexane is readily sensed while cyclohexane is not, probably because of size exclusion by the small portal size for ZIF-8 cavities. The sensor is unresponsive to water vapor but can detect ethanol. The ethanol-concentration-dependent responses were used to determine the ethanol concentrations in ethanol/water mixtures with the sensor response saturating at ca. 40% ethanol (Figure 1c,e).

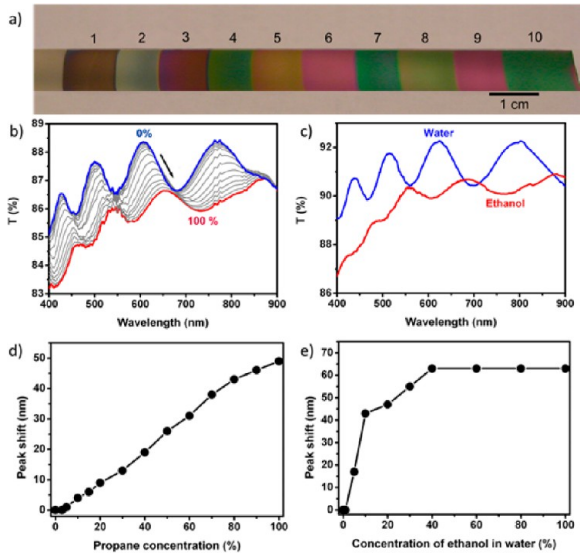

Figure 1. (a) Photograph of a series of ZIF-8 films of various thicknesses grown on silicon substrates. UV−vis transmission spectra of a ZIF-8 film on glass after exposure to (b) propane vapor of various concentrations from 0% (blue) to 100% (red) and (c) ethanol (red) or water (blue) and corresponding interference peak (originally at 612 nm) shift versus (d) propane concentration in N_2 diluent and (e) ethanol concentration (v/v %) in ethanol/water solutions. Copyright 2010 American Chemistry Society.

Such effects were also observed in other vapor-sensing MOFs. Li and co-workers reported a microporous $[Zn_2(bpdc)_2(bpee)]$ MOF (bpdc = 4,4′-biphenyldicarboxylate; bpee = 1,2-bipyridylethene) for explosive sensing.[38] The framework fluorescence can be quenched by analogues of explosive molecules such as 2,4-dinitrotoluene (DNT) and 2,3-dimethyl-2,3-dinitrobutane (DMNB) through a redox-quenching mechanism (Figure 2). The pore-size confinement leads to the enhancement of DMNB quenching, as is reflected by the relatively small difference in the quenching percentages for nitrobenzene and DMNB despite the fact that nitrobenzene should have elicited larger fluorescence quenching owing to its much higher vapor pressure, more favorable reduction potential, and stronger $\pi-\pi$ interactions with the framework.

MOFs can also be combined with other sensing structures to enhance sensor performances. For instance, by coating noble-metal nanoparticles with MOFs, both selectivity and sensitivity of gas sensing could be enhanced dramatically.[26,29]

Luminescent Ion Sensing via Coordination or Hydrogen Bonding to MOFs. Vacant binding sites in the MOF framework can be utilized to elicit selectivity in ion sensing. For metal-cation sensing, Lewis basic centers within porous MOFs are desired. Envisioning preferential binding of Ln^{3+} ions to

dx.doi.org/10.1021/ic402194c | Inorg. Chem. 2014, 53, 1916−1924

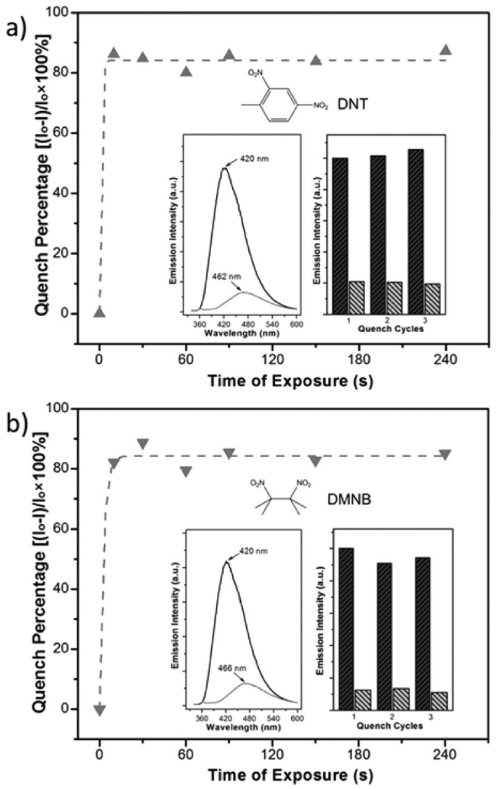

Figure 2. Time-dependent fluorescence quenching by (a) DNT and (b) DMNB (excitation wavelength = 320 nm). Insets: corresponding fluorescence spectra before and after exposure to the analyte vapors for 10 s (left) and three consecutive quench/regeneration cycles (right). Copyright 2009 Wiley-VCH.

carboxylate oxygen atoms over pyridyl nitrogen atoms, Chen et al. prepared an Eu-pdc MOF (pdc = pyridine-3,5-dicarboxylate) with dangling Lewis basic pyridyl sites for the sensing of metal ions (Figure 3).[39] After activation in *N*,*N*-dimethylformamide

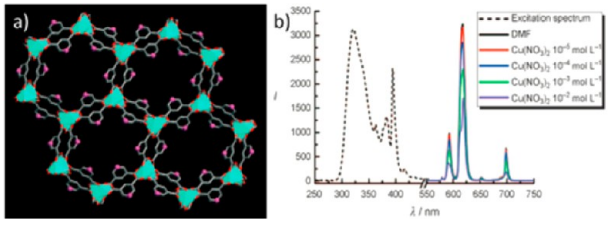

Figure 3. (a) Crystal structure of the Eu-pdc MOF, viewed along the *a* axis. (b) Excitation and photoluminescence spectra of MOF activated in DMF solutions of $Cu(NO_3)_2$ at different concentrations (excited and monitored at 321 and 618 nm, respectively). Copyright 2009 Wiley-VCH.

(DMF) solutions of the metal ions, the $[Eu(pdc)_{1.5}]\cdot DMF$ MOF shows luminescence quenching response selectively to ions such as Cu^{2+}, Mn^{2+}, or Co^{2+}. The quenching is suggested to result from the weak binding of pyridyl nitrogen atoms to M^{2+}, which reduces the energy-transfer efficiency of the pdc organic linkers to the f–f transitions of Eu^{3+}.

Jiang et al. used a different route for cation recognition.[40] They synthesized $[Pb_2(bco)_2(bipy)]$ [bco = 1,5-bis(*m*-carboxyphenoxy)-3-oxapentane and bipy = 4,4′-bipyridine], from which the weakly coordinating bipy can be leached out postsynthetically (Figure 4). After removal of the bipy ligand,

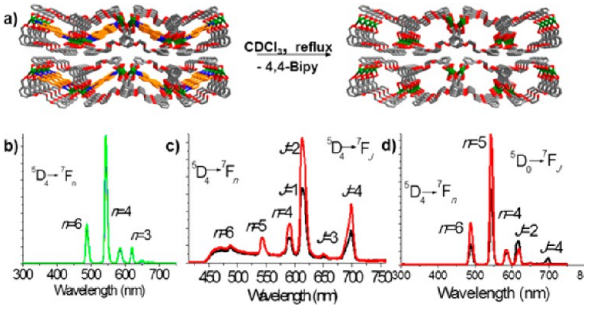

Figure 4. (a) Schematic showing the formation of $[Pb_2(bco)_2]$ by leaching of the weakly coordinating bipy. The cation encapsulation and exchange experiments give the emission spectra of (b) after stirring $[Pb_2(bco)_2]$ in $Tb(ClO_4)_3$ aqueous solution for 3 h. (c) Sample of part b stirred in $Eu(ClO_4)_3$ aqueous solution at 1 (black) and 2 (red) days. (d) Sample of part c stirred in $Tb(ClO_4)_3$ aqueous solution at 1 (black) and 2 (red) days. Excitations are all at 303 nm. Copyright 2009 Wiley-VCH.

the resulting hydrophilic channels can reversibly encapsulate $[Ln(H_2O)_8]^{3+}$ ions. The confined oxygen-rich environment induces host–guest O–H···O hydrogen-bonding interactions that reduces the O–H vibration coupling on $[Ln(H_2O)_8]^{3+}$ ions, resulting in much higher emission intensity after entrapment.

Hydrogen bonding was utilized by Chen et al. for anion recognition and sensing with MOFs. They reported a luminescent Tb(BTC)·G (BTC = benzene-1,3,5- tricarboxylate, G = guest solvent) MOF as an anion sensor that exhibits high sensitivity and selectivity for fluoride (Figure 5).[41] The

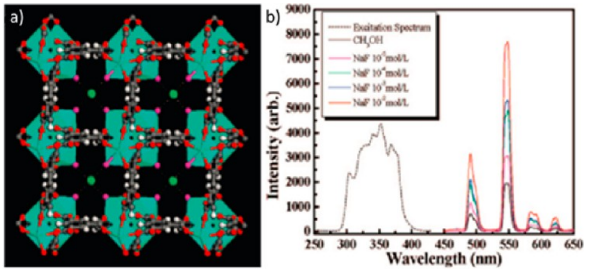

Figure 5. (a) Single-crystal X-ray structure of a Tb(BTC) MOF activated in methanol containing NaF. (b) Excitation (dotted) and photoluminescence spectra (solid) of the Tb(BTC) MOF activated in different concentrations of NaF. Copyright 2008 American Chemistry Society.

luminescence intensity of Tb(BTC)·methanol was enhanced after anion incorporation: the F^--incorporated MOF showed a 4 times stronger luminescence signal than the non-F^- counterpart (Figure 5b). The luminescence enhancement was proposed to result from hydrogen bonding of F^- to terminal methanol, as indicated by F^-···O (from methanol) distances of 2.78–3.24 Å (Figure 5a). Such a strong hydrogen-bonding interaction alleviates the quenching effect of the O–H bond stretching vibrations, thereby leading to luminescence enhancement. A recent report by Song and co-workers described luminescence turn-on sensing of DMF vapor by Eu-MOF using a similar strategy.[30]

Analyte-Specific Signal Response for Selective Sensing. For accurate and quantitative sensing, a sensory material that responds to specific molecules is desired. Lin and co-workers reported a highly phosphorescent MOF series based

dx.doi.org/10.1021/ic402194c | Inorg. Chem. 2014, 53, 1916–1924

on $Ir(ppy)_3$ (ppy = 2-phenylpyridine) derivatives that can be readily quenched by oxygen (Figure 6).[42] Linear Stern–Völmer

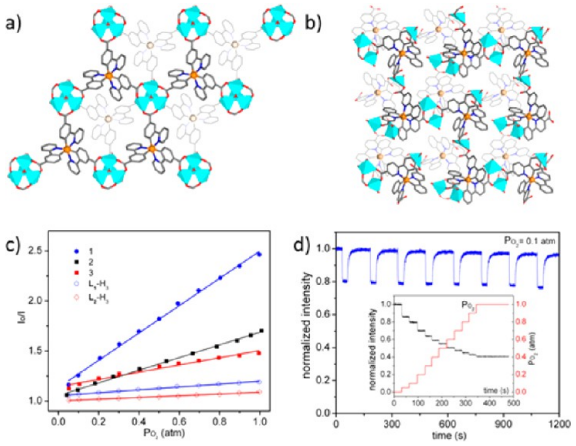

Figure 6. Top view of the 2D bilayer structure of the MOFs synthesized from two $Ir(ppy)_3$-derived ligands (a and b). (c) Stern–Volmer plot showing I_0/I vs O_2 partial pressure for ligand complexes and MOFs. (d) Reversible quenching of phosphorescence of the MOF upon alternating exposure to 0.1 atm of O_2 and application of a vacuum. The inset shows rapid equilibration of phosphorescence of the MOF after each dose of O_2. Copyright 2010 American Chemistry Society.

plots of I_0/I vs $p(O_2)$ (oxygen partial pressure) were obtained, and the reversibility of luminescent quenching was evaluated by examining the emission intensity change when $p(O_2)$ was cycled between 0 and 0.1 atm (Figure 6c,d). It was found that a permanent porosity is required for kinetically reversible O_2 quenching. In this sensing scheme, the microporosity of MOFs can impart additional selectivity as large interfering molecules are excluded from quenching the MOF luminescence. Chen and co-workers adopted the same principle to design ruthenium-doped azolate MOF for oxygen sensing.[43,44]

Host–Guest Chemistry in Entangled Frameworks for Molecular Decoding. Although many sensory MOFs have been reported, a few of them can distinguish similar analytes because of the fact that these MOF materials transduce the intensity of only one kind of signal. An interesting MOF system was developed by Kitagawa and co-workers to decode multiple analytes by transducing a particular host–guest interaction into corresponding luminescent signals (Figure 7a).[45] $[Zn_2(bdc)_2(dpNDI)]_n$ (bdc = 1,4-benzenedicarboxylate; dpNDI = *N*,*N*′-di-4-pyridyl-1,4,5,8-naphthalenediimide) possesses an entangled structure, which is believed to be crucial for signal transduction. Upon uptake of aromatic volatile organic compounds, the entangled framework shows a crystal-to-crystal transition from distorted to nondistorted structure, accompanied by a strong analyte-specific fluorescence signal (Figure 7b–d). Two analyte-specific fluorescence turn-on mechanisms were proposed: charge-transfer emission and heavy-atom-induced phosphorescence enhancement. The signal response is enhanced by the host–guest interaction but is nonlinear with respect to the concentration of the guest molecules.

Chiral MOF for Enantioselective Sensing. Rapid determination of enantiomeric excesses (ee) of organic compounds has become a bottleneck in identifying efficient means to produce chiral molecules. Lin and co-workers hypothesized that chiral MOFs can provide an excellent platform for enantioselective sensing by taking advantage of

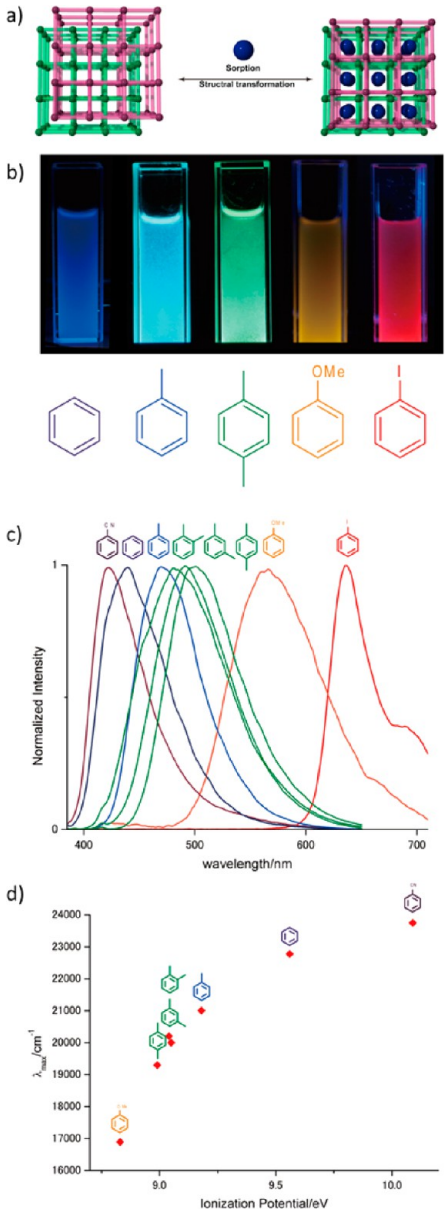

Figure 7. (a) Schematic depiction of space flexibility in entangled MOF for molecular decoding. (b) Resulting luminescence of a MOF powder suspension in the organic liquid indicated with 365 nm irradiation. (c) Normalized luminescent spectra of guest-containing MOFs upon excitation at 370 nm. (d) Relationship between the emission energy of a guest-containing MOF and the ionization potential of each guest molecule. Copyright 2011 Nature Publishing Group.

the confinement effect of the framework and the conformational rigidity of the sensing moieties to enhance stereoselectivity.[46] A BINOL-based chiral porous MOF, $[Cd_2(L)(H_2O)_2]\cdot 6.5DMF\cdot 3EtOH$ [LH_4 = (*R*)-2,2′-dihydroxy-1,1′-binaphthyl-4,4′,6,6′-tetrakis(4-benzoic acid)], was tested as an enantioselective sensor for amino alcohols via fluorescence quenching (Figure 8a).[46] The MOF gives much higher detection sensitivity (up to 1000-fold) and greater enantioselectivity compared with the homogeneous control. For 2-amino-3-methyl-1-butanol (AA), the MOF has a quenching ratio [QR = $k_{SV}(S)/k_{SV}(R)$] of 3.12, while the homogeneous control has a QR of 1.21 (Figure 8b). The increase of sensitivity is believed to result from a preconcentration effect, as proven

dx.doi.org/10.1021/ic402194c | *Inorg. Chem.* 2014, 53, 1916–1924

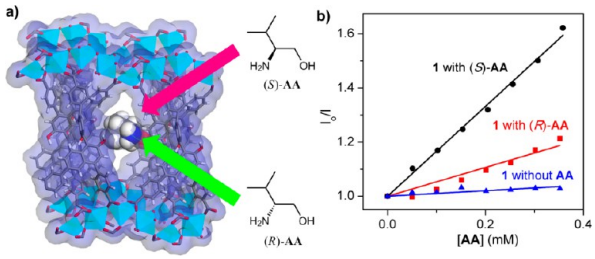

Figure 8. (a) Schematic showing chiral sensing of amino alcohols with a Cd-MOF with a BINOL-derived tetracarboxylate ligand. (b) Stern–Völmer plots of fluorescence quenching of the Cd-MOF by (*R*)- and (*S*)-AA. Copyright 2012 American Chemical Society.

by determination of the solubility partition coefficient in the MOF and acetonitrile by gas chromatographic analyses. The enantioselectivity enhancement of the AA substrate is likely caused by steric confinement of the MOF cavity. The MOF sensor was also shown to be capable of determining the enantiomeric ratio of a mixture of (*S*)- and (*R*)-AA in predetermined proportions by comparing it with the calibration curve, which exhibits a linear relationship between the fluorescence signal and the ee of the analyte. This work demonstrates that chiral porous MOFs can provide an excellent platform for developing practically useful chiral sensors.

MOFS AS IMAGING AGENTS

Despite enormous progress in our fundamental understanding of cancer biology, the mortality rate for most cancers has remained unchanged over the past 2–3 decades.[47] It has long been recognized that early detection is the key for the effective treatment of cancer. Unfortunately, many patients are still diagnosed at late stages of cancer because of limited sensitivity and selectivity of current diagnostic techniques.[48] Conventional diagnostic agents, such as Gd^{3+} chelates for MRI and iodinated aromatic molecules for CT imaging, are limited by their short blood circulation times and nonspecific biodistribution. In an attempt to overcome these limitations, various nanoparticle platforms have been developed for cancer diagnostics. Nanoparticles in the size range of 10–100 nm provide several potential advantages over conventional small-molecule agents, including extension of circulating half-lives, passive accumulation at tumor sites because of the EPR effect, active targeting of cancer cells, and improved safety profiles.[49]

Lin and co-workers have developed systematic strategies to scale down MOFs to the nanoregime to form crystalline NMOFs or amorphous nanoscale coordination polymers (NCPs) for imaging and drug delivery.[50] A variety of different techniques, including nanoprecipitation,[13] solvothermal,[51] reverse microemulsion,[52] and surfactant-templated solvothermal reactions, have been developed to synthesize NMOFs and NCPs.[53] Biomedically relevant agents were loaded into NMOFs or NCPs using two general strategies, either by integrating active agents into the frameworks directly (Scheme 1a)[54,55] or by loading active agents into the pores and channels of the NMOFs (Scheme 1b).[14,51,56–58] The surfaces of as-synthesized NMOF and NCP particles were modified with a thin shell of silica,[59–61] organic polymers [e.g., poly(ethylene glycol) (PEG) and poly(vinylpyrrolidone) (PVP)],[13,54,61,62] or lipid bilayers[12,63] in order to enhance their stabilities, fine-tune their physicochemical properties, and impart additional biocompatibility and functionality. A number of NMOFs and

Scheme 1. Schematic Representations of Direct Incorporation of Biomedically Relevant Agents into the MOF Framework (a) and Cargo Loading by Noncovalent (b1) and Covalent (b2) Means

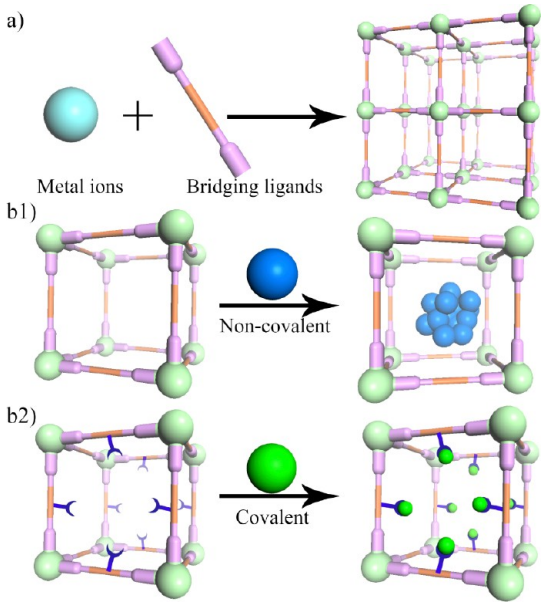

NCPs have been tested as biomedical imaging agents in vitro and in vivo.

NMOFs for MRI. MRI is a noninvasive imaging technique whereby images are generated based on the NMR signals of the water proton (^1H) nuclei in a specimen. MRI is a powerful imaging modality with high spatial resolution and depth of penetration. However, their low sensitivity requires that a relatively large amount of contrast agent be administered to provide adequate MRI contrast. Lin and co-workers explored NMOFs as MRI contrast agents by taking advantage of the large payloads of paramagnetic metal ions that NMOFs can carry. Both Gd^{3+}- and Mn^{2+}-containing NMOFs were shown to serve as excellent T_1-weighted MRI contrast agents with large per metal-based and per particle-based MRI relaxivities.[53,54]

NMOFs of $Gd(BDC)_{1.5}(H_2O)_2$ and $[Gd(1,2,4\text{-BTC})(H_2O)_3]H_2O$ were synthesized by stirring an optically transparent microemulsion of $GdCl_3$ and bis(methylammonium)-benzene-1,4-dicarboxylate (BDC) or tris(methylammonium)-benzene-1,2,4-tricarboxylate (1,2,4-BTC) in the cationic cetyltrimethylammonium bromide/isooctane/1-hexanol/water system.[52] Surfactant molecules played an important role in defining NMOF morphologies. By variation of the water/surfactant molar ratio (W value) and reaction time, distinct particle morphologies were obtained. This reverse microemulsion-based synthetic methodology was general and applied to many other NMOF and NCP systems. Extraordinarily large longitudinal relaxivity ($r_1 = 1.6 \times 10^7$ mM^{-1} s^{-1}) and transverse relaxivity ($r_2 = 2.5 \times 10^7$ mM^{-1} s^{-1}) on a per millimolar of nanoparticle basis were obtained for $Gd(BDC)_{1.5}(H_2O)_2$ because of the large amount of Gd^{3+} centers carried by each particle (Figure 9a). Highly luminescent europium- and terbium-doped $Gd(BDC)_{1.5}(H_2O)_2$ nanoparticles were also synthesized by adding a small amount (5 mol %) of Eu^{3+} or Tb^{3+} into the Gd-NMOF synthesis to render them potentially useful as multimodal imaging agents (Figure 9b).

The above-mentioned Gd-NMOFs were modified with PVP and then coated with a thin shell of silica in order to control the

dx.doi.org/10.1021/ic402194c | Inorg. Chem. 2014, 53, 1916–1924

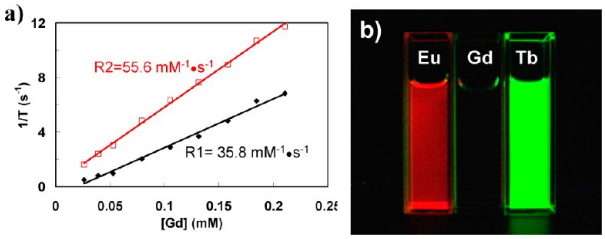

Figure 9. (a) r_1 and r_2 relaxivity curves of $Gd(BDC)_{1.5}(H_2O)_2$ of ~100 nm length by ~40 nm diameter. In comparison, OmniScan gave an r_1 of 4.1 mM^{-1} s^{-1} under these conditions. (b) Luminescence images of ethanolic suspensions of europium- and terbium-doped $Gd(BDC)_{1.5}(H_2O)_2$ when irradiated with UV light. Copyright 2006 American Chemical Society.

release of Gd^{3+} ions.[61] The thickness of the silica shell could be controlled precisely by tuning the base concentration and reaction time. Silica coatings on nanoparticles can improve water dispersibility, biocompatibility, and the ability to further functionalize the shell through co-condensation of siloxy-derived moieties. It was shown that the silica coating retarded the release of cargos from NMOFs, presumably as a result of the slow diffusion rate of metal and organic constituents through the silica shell. To illustrate the utility of NMOF-based core–shell nanostructures, europium-doped $Gd(BDC)_{1.5}(H_2O)_2@SiO_2$ was prepared and the silica surface was further functionalized with a silylated Tb-EDTA monoamide derivative. Ratiometric luminescence sensing of dipicolinic acid (DPA), a chemical marker for anthrax spore, with a detection limit as low as 48 nM was achieved because of the optical signals generated from the binding of DPA to terbium complexes on the nanoparticle surface.

Lin and co-workers also reported the synthesis of two new Gd-NMOFs, $[Gd_2(bhc)(H_2O)_6]$ (bhc = benzenehexacarboxylate) and $[Gd_2(bhc)(H_2O)_8](H_2O)_2$ using a surfactant-assisted technique at elevated temperatures.[53] The two different NMOFs based on the identical gadolinium and bhc building blocks result from different metal–ligand coordination modes. The potential of these NMOFs as MRI contrast agents was demonstrated by a relaxivity study, wherein a modest r_1 of 1.5 mM^{-1} s^{-1} and an impressive r_2 of 122.6 mM^{-1} s^{-1} on a per gadolinium basis were obtained. Because of the high gadolinium payloads in these particles, the r_1 and r_2 relaxivities on a per particle basis were determined to be 8.36×10^5 and 6.83×10^7 mM^{-1} s^{-1}, respectively.

The toxicity associated with Gd^{3+} leaching hinders the in vivo applications of Gd-NMOFs as MRI contrast agents. To overcome this issue, Lin and co-workers designed NMOFs using Mn^{2+} as the metal-connecting points to afford T_1-weighted MRI-enhancing agents that are more biocompatible and less toxic.[54] $Mn(BDC)(H_2O)_2$ and $Mn_3(BTC)_2(H_2O)_6$ were synthesized by reacting terephthalic acid (BDC) and trimesic acid (BTC) with $MnCl_2$ in reverse-phase microemulsions, respectively.[54] These particles were coated with a thin silica shell, and their surfaces were subsequently functionalized with a cyclicarginine-glycine-aspartate (RGD) peptide for tumor-specific targeting. The Mn-NMOFs were shown to be highly efficient T_1-weighted MRI contrast agents in vitro because of their ability to carry a large payload of Mn^{2+} and subsequent release of Mn^{2+} upon NMOF decomposition. Increased uptake of the cRGD targeted particles was confirmed by in vitro MRI, confocal microscopy, and inductively coupled plasma mass spectrometry (ICP-MS) studies (Figure 10).

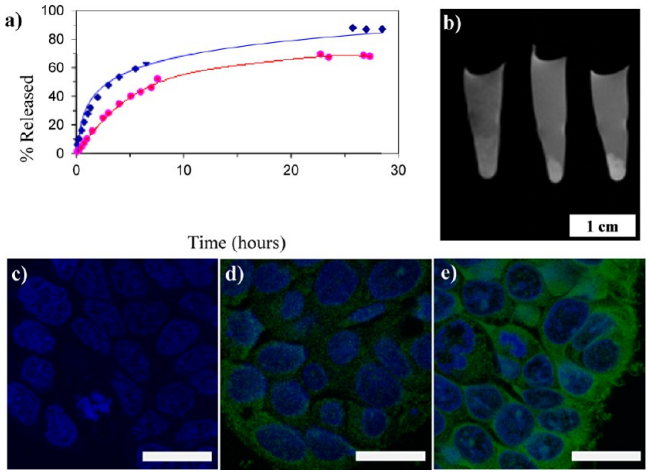

Figure 10. (a) Dissolution curves of uncoated (blue) and silica-coated (red) $Mn_3(BTC)_2(H_2O)_6$ nanoparticles ($Mn@SiO_2$) in water at 37 °C (% released vs time). (b) In vitro MRI images of HT-29 cells incubated with no particle (left), nontargeted $Mn@SiO_2$ (middle), and c(RGDfK)-targeted $Mn@SiO_2$ (right). (c–e) Merged confocal images of HT-29 cells that were incubated with no particles (c), nontargeted $Mn@SiO_2$ (d), and c(RGDfK)-targeted $Mn@SiO_2$ (e). The blue color was from DRAQ5 used to stain the cell nuclei, while the green color was from rhodamine B. The bars represent 20 μm. Copyright 2008 American Chemical Society.

Iron-based NMOFs of the MIL structures were shown to be efficient contrast agents for T_2-weighted MRI imaging.[14] The PEGylated MIL-88 nanoparticles exhibited an r_2 relaxivity of 50 mM^{-1} s^{-1} at 9.4 T. In vivo MRI imaging of Wistar female rats 30 min after nanoparticle injection showed enhanced contrast in the liver and spleen (Figure 11). In a separate study where biodistribution, metabolism, and excretion of iron-based NMOFs was investigated in rats after intravenous injections,

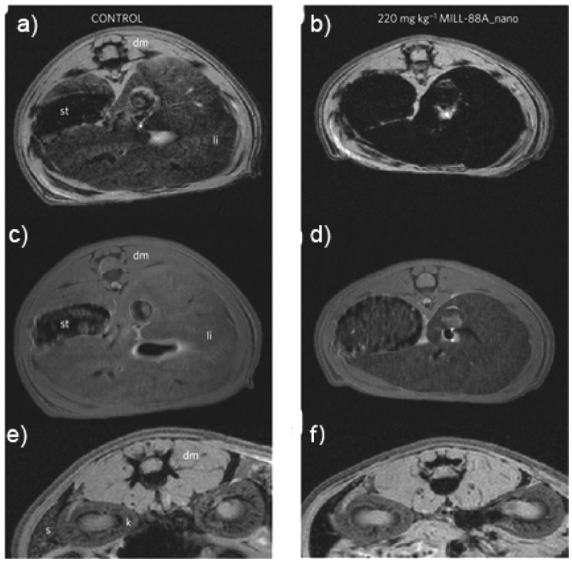

Figure 11. T_2-weighted MRI images of Wistar rats injected with no particle (a, c, and e) or 220 mg/kg MIL-88A (e, d, and f). The images were acquired using either gradient-echo (a, b, e, and f) or spin-echo (c and d) sequences. The images show the liver (a–d) or spleen (e and f) regions 30 min postinjection (dm = dorsal muscle, k = kidney, li = liver, s = spleen, st = stomach). Reproduced with permission from ref 14. Copyright 2010 Nature Publishing Group.

dx.doi.org/10.1021/ic402194c | Inorg. Chem. 2014, 53, 1916–1924

Horcajada and co-workers showed that iron-based NMOFs did not lead to any acute toxicity in rats after high doses of these nanoparticles, thus supporting the potential usage of iron-based NMOFs for biomedical applications.[64]

NMOFs for CT Imaging. By incorporating high-Z-element building blocks, NMOFs have also been tested as contrast agents for X-ray CT imaging.[55] Iodinated NMOFs of the formulas $[Cu(I_4\text{-BDC})(H_2O)_2]\cdot 2H_2O$ and $[Zn(I_4\text{-BDC})(EtOH)_2]\cdot 2EtOH$ were prepared using 2,3,4,5,6-tetraiodo-1,4-benzenedicarboxylate (I_4-BDC) as the bridging ligands and Cu^{2+} and Zn^{2+} as the metal connecting points. These NMOFs carry exceptionally high iodine content (up to 63 wt %). As shown in Figure 12, phantom studies indicated that these

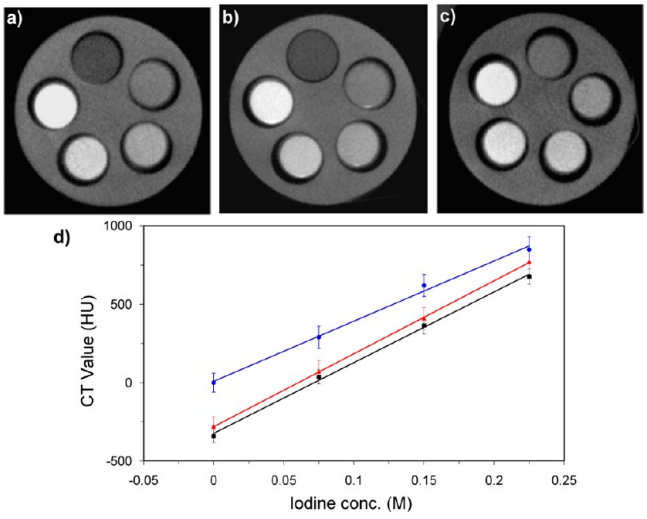

Figure 12. CT phantom images of (a) $[Cu(I_4\text{-BDC})(H_2O)_2]\cdot 2H_2O$ (NCP 3a) and (b) $[Zn(I_4\text{-BDC})(EtOH)_2]\cdot 2EtOH$ (NCP 5b) dispersed in ethanol, and (c) Iodixanol in aqueous solution. From the top, clockwise, the slots have [I] = 0, 0.075, 0.150, 0.225, and 0.300 M. (d) X-ray attenuation as a function of [I] for NCP 3a at 40 kVp, NCP 5b at 50 kVp, and Iodixanol at 40 kVp. Blue: Iodixanol. Red: NCP 3a. Black: 5b. Copyright 2009 Wiley-VCH.

particles have X-ray attenuation coefficients comparable to that of the molecular contrast agent (Iodixanol). NMOFs thus provide a novel platform for the design of efficient CT contrast agents by incorporating iodinated bridging ligands.

More recently, Lin and co-workers prepared Zr-BDC and Hf-BDC NMOFs of the UiO-66 structure. These particles carry 37 wt % Zr and 57 wt % Hf, respectively. The Hf-NMOF was twice as efficient in attenuating X-rays as Iodixanol, resulting from the higher X-ray attenuation coefficient of Hf compared to I. The Hf-BDC NMOF was further coated with silica and PEG and examined as a contrast agent for in vivo CT imaging of mice.[65] Enhanced attenuation in the liver (+131 HU) and spleen (+86 HU) was observed in mice 15 min after intravenous injection (Figure 13). The NMOF platform thus provides a promising strategy for incorporating high loadings of heavy elements into nanoparticles that can be surface-functionalized for enhanced biocompatibility and in vivo performance.

NCPs for OI. OI is another powerful imaging modality for detecting tumor and other diseased tissues because of their noninvasive nature and higher sensitivity compared to MRI and CT. Organic-dye-loaded nanoparticles and luminescent quantum dots are two major nanoprobes for OI. The former can

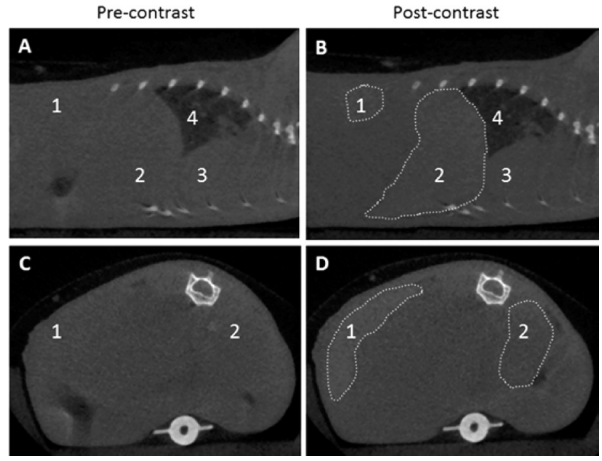

Figure 13. (A and B) Sagittal and (C and D) axial CT slices of a mouse precontrast and 15 min after injection of Hf-UiO@SiO_2@PEG. The areas of increased attenuation are outlined, and the labels are as follows: 1, spleen (+131 HU); 2, liver (+86 HU); 3, heart; 4, lungs. Copyright 2012 Royal Society of Chemistry.

suffer from self-quenching and photobleaching, whereas the latter can have high toxicity. To overcome these problems, Lin and co-workers hypothesized that highly luminescent nanoparticles can be constructed from metal complexes whose luminescence originates from the triplet states with long lifetimes and large Stokes shifts.[66] Such luminescent nanoparticles will not undergo self-quenching even at very high dye loadings. Phosphorescent NCPs were synthesized using a carboxylic acid derivative of $Ru(bpy)_3^{2+}$ (bpy = 2,2′-bipyridine) as a bridging ligand and Zn^{2+} or Zr^{4+} metal-connecting points (Figure 14a).[66] The Zn- and Zr-NCPs have extremely high $Ru(bpy)_3^{2+}$ dye loadings of 78.7% and 57.4%, respectively. The Zr-NCP was further stabilized with a thin shell of amorphous

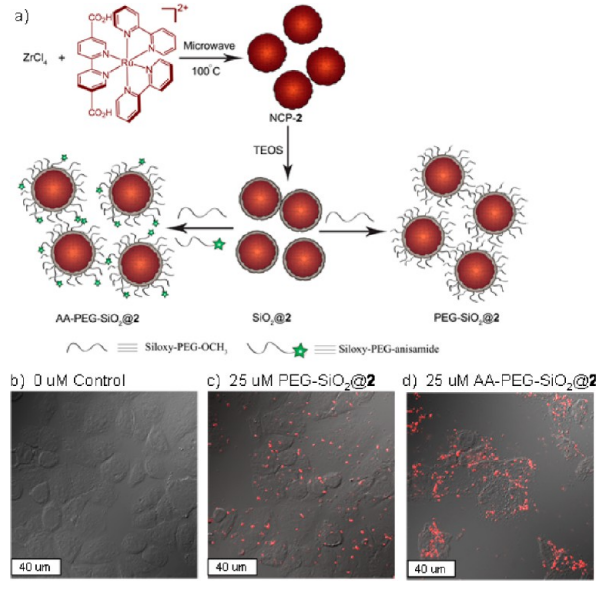

Figure 14. (a) Synthesis of Zr-NCP, coating of Zr-NCP with silica, and further functionalization with PEG and PEG−anisamide. Confocal microscopic images of H460 cells that have been incubated with various nanoparticles: control cells without any particles (b), cells with Zr-NCP@PEG-SiO_2 (c), and cells with Zr-NCP@AA-PEG-SiO_2 (d). Copyright 2011 Wiley-VCH.

dx.doi.org/10.1021/ic402194c | Inorg. Chem. 2014, 53, 1916−1924

silica to prevent rapid dye release from the nanoparticles, and the biocompatibility and targeting efficiency of the NCP/silica core−shell nanostructures were further improved by coating with PEG and PEG−anisamide. Enhanced contrast and uptake was confirmed by laser scanning confocal fluorescence microscopy and particle uptake studies using H460 lung cancer cells (Figure 14b).

Kimizuka and co-workers synthesized NCPs based on nucleotide and lanthanide ion building blocks.[67] Fluorescent dyes and many other functional molecules can be readily encapsulated into nanoparticles during the NCP synthesis. Fluorescent dyes in these nanoparticles have higher quantum yields compared to free dyes in solid form with a single-exponential decay, showing that guest molecules are monomerically wrapped in the network (Figure 15). Adsorption of

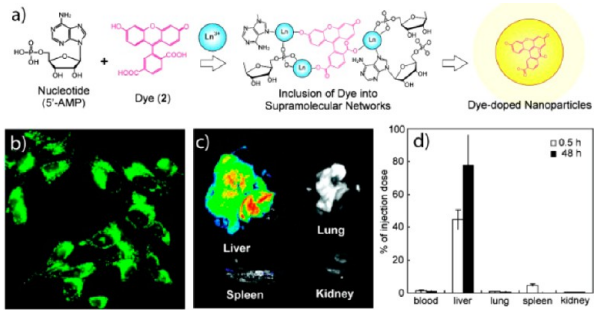

Figure 15. (a) Schematic representation of the incorporation of anionic dyes within supramolecular networks. (b) Fluorescence microscopy image of HeLa cells incubated with 4-doped 5′-AMP/Gd^{3+} NPs. (c) Fluorescent images of organs from mice injected with 4-doped 5′-AMP/Gd^{3+} NPs. (d) Biodistribution of 4-doped 5′-AMP/Gd^{3+} NPs in mice at 0.5 and 48 h postinjection time points. Copyright 2009 American Chemical Society.

polyelectrolytes on nanoparticle surfaces was shown to improve their water solubility and biocompatibility. However, a biodistribution study using fluorescence imaging and ICP-MS showed that these particles were rapidly captured by liver in mice after intravenous injection. Nevertheless, the adaptive nature of this NCP platform provides a facile means for incorporating and delivering functional cargoes.

CONCLUSION AND OUTLOOK

As outlined in this Forum Article, MOFs have emerged as a promising platform for chemical sensing and biological/biomedical imaging. Several unique properties of MOFs have been utilized for their specific recognition of small molecules or ions in chemical sensing. The tunability of the MOF synthesis should allow the design of the next generation of MOF sensors that exhibit excellent sensitivity, by taking advantage of the preconcentration effect of the pores and channels in MOFs, and enhanced selectivity, as a result of well-defined pores and channels and the framework rigidity in MOFs. In order to move MOF sensors into the realm of practical applications, a number of issues need to be addressed: (1) chemical and mechanical stabilities of many MOF sensors need to be increased; (2) more general approaches are needed to prepare MOF thin films of controlled thicknesses; (3) reliable methods are needed to integrate MOFs into other device structures to facilitate signal transduction and readout; (4) costs for MOF sensor production need to be minimized. Nevertheless, the area of chemical sensing with MOFs will continue to flourish, and practically useful MOF sensors will appear in the near future.

In comparison to MOF sensors, NMOFs and NCPs are less explored for biological and biomedical imaging. They have been examined as contrast agents for MRI, CT, and OI. The ability to readily tune compositions, particle sizes and morphologies, and surface functionalities makes NMOFs/NCPs a unique class of hybrid nanomaterials for biomedical applications, particularly in the early diagnosis of cancer. NMOFs/NCPs are potentially advantageous over other inorganic nanoparticles owing to their intrinsic biodegrability of NMOFs/NCPs and the ability to use biocompatible building blocks. In addition, surface functionalization of NMOFs/NCPs with stealth coating and cell-targeting ligands should endow their long blood circulation and selective tumor targeting capabilities. The compositional and structural diversity of NMOFs/NCPs should also make it possible to codeliver imagining contrast agents and chemotherapeutic drugs to provide real-time monitoring of cargo delivery and tumor response to treatment. Significant efforts are needed to critically evaluate NMOFs/NCPs in vivo to establish preclinical guidelines on their efficacy and safety. NMOFs/NCPs are expected to have a bright future in biomedical imaging.

AUTHOR INFORMATION

Corresponding Author

*E-mail: wenbinlin@uchicago.edu.

Notes

The authors declare no competing financial interest.

ACKNOWLEDGMENTS

We thank the NSF (Grant DMR-0906662) and NIH-NCI (Grant U01-CA151455) for financial support.

REFERENCES

(1) Ma, L.; Falkowski, J. M.; Abney, C.; Lin, W. *Nat. Chem.* **2010**, *2*, 838−846.
(2) Lee, J.; Farha, O. K.; Roberts, J.; Scheidt, K. A.; Nguyen, S. T.; Hupp, J. T. *Chem. Soc. Rev.* **2009**, *38*, 1450−1459.
(3) Ma, L.; Abney, C.; Lin, W. *Chem. Soc. Rev.* **2009**, *38*, 1248−1256.
(4) Song, F.; Wang, C.; Falkowski, J. M.; Ma, L.; Lin, W. *J. Am. Chem. Soc.* **2010**, *132*, 15390−15398.
(5) Wu, C.-D.; Hu, A.; Zhang, L.; Lin, W. *J. Am. Chem. Soc.* **2005**, *127*, 8940−8941.
(6) Furukawa, H.; Ko, N.; Go, Y. B.; Aratani, N.; Choi, S. B.; Choi, E.; Yazaydin, A. O.; Snurr, R. Q.; O'Keeffe, M.; Kim, J.; Yaghi, O. M. *Science* **2010**, *329*, 424−428.
(7) Ma, L.; Mihalcik, D. J.; Lin, W. *J. Am. Chem. Soc.* **2009**, *131*, 4610−4612.
(8) Murray, L. J.; Dinca, M.; Long, J. R. *Chem. Soc. Rev.* **2009**, *38*, 1294−1314.
(9) Uemura, K.; Kitagawa, S.; Fukui, K.; Saito, K. *J. Am. Chem. Soc.* **2004**, *126*, 3817−3828.
(10) Evans, O. R.; Lin, W. *Acc. Chem. Res.* **2002**, *35*, 511−522.
(11) Kent, C. A.; Mehl, B. P.; Ma, L.; Papanikolas, J. M.; Meyer, T. J.; Lin, W. *J. Am. Chem. Soc.* **2010**, *132*, 12767−12769.
(12) Huxford, R. C.; deKrafft, K. E.; Boyle, W. S.; Liu, D.; Lin, W. *Chem. Sci.* **2012**, *3*, 198−204.
(13) Rieter, W. J.; Pott, K. M.; Taylor, K. M. L.; Lin, W. *J. Am. Chem. Soc.* **2008**, *130*, 11584−11585.
(14) Horcajada, P.; Chalati, T.; Serre, C.; Gillet, B.; Sebrie, C.; Baati, T.; Eubank, J. F.; Heurtaux, D.; Clayette, P.; Kreuz, C.; Chang, J.-S.; Hwang, Y. K.; Marsaud, V.; Bories, P.-N.; Cynober, L.; Gil, S.; Ferey, G.; Couvreur, P.; Gref, R. *Nat. Mater.* **2010**, *9*, 172−178.
(15) Chen, Z.; Lu, C. *Sens. Lett.* **2005**, *3*, 274−295.

(16) Li, J.; Lu, Y.; Ye, Q.; Cinke, M.; Han, J.; Meyyappan, M. *Nano Lett.* **2003**, *3*, 929−933.
(17) Kolmakov, A.; Moskovits, M. *Annu. Rev. Mater. Res.* **2004**, *34*, 151−180.
(18) Thakar, R.; Chen, Y.; Snee, P. T. *Nano Lett.* **2007**, *7*, 3429−3432.
(19) Burns, A.; Sengupta, P.; Zedayko, T.; Baird, B.; Wiesner, U. *Small* **2006**, *2*, 723−726.
(20) Kong, J.; Franklin, N. R.; Zhou, C.; Chapline, M. G.; Peng, S.; Cho, K.; Dai, H. *Science* **2000**, *287*, 622−625.
(21) Heath, J. R.; Davis, M. E. *Annu. Rev. Med.* **2008**, *59*, 251−265.
(22) Cheng, M. M.-C.; Cuda, G.; Bunimovich, Y. L.; Gaspari, M.; Heath, J. R.; Hill, H. D.; Mirkin, C. A.; Nijdam, A. J.; Terracciano, R.; Thundat, T.; Ferrari, M. *Curr. Opin. Chem. Biol.* **2006**, *10*, 11−19.
(23) Sun, Y.; Rogers, J. A. *Adv. Mater.* **2007**, *19*, 1897−1916.
(24) Shipway, A. N.; Katz, E.; Willner, I. *ChemPhysChem* **2000**, *1*, 18−52.
(25) Lin, P.; Yan, F. *Adv. Mater.* **2012**, *24*, 34−51.
(26) Mabeck, J.; Malliaras, G. *Anal. Bioanal. Chem.* **2006**, *384*, 343−353.
(27) Yavuz, M. S.; Cheng, Y.; Chen, J.; Cobley, C. M.; Zhang, Q.; Rycenga, M.; Xie, J.; Kim, C.; Song, K. H.; Schwartz, A. G.; Wang, L. V.; Xia, Y. *Nat. Mater.* **2009**, *8*, 935−939.
(28) Lee, J. E.; Lee, N.; Kim, H.; Kim, J.; Choi, S. H.; Kim, J. H.; Kim, T.; Song, I. C.; Park, S. P.; Moon, W. K.; Hyeon, T. *J. Am. Chem. Soc.* **2010**, *132*, 552−557.
(29) Cheon, J.; Lee, J.-H. *Acc. Chem. Res.* **2008**, *41*, 1630−1640.
(30) Peer, D.; Karp, J. M.; Hong, S.; Farokhzad, O. C.; Margalit, R.; Langer, R. *Nat. Nanotechnol.* **2007**, *2*, 751−760.
(31) Fang, J.; Nakamura, H.; Maeda, H. *Adv. Drug Delivery Rev.* **2011**, *63*, 136−151.
(32) Ferrari, M. *Nat. Rev. Cancer* **2005**, *5*, 161−171.
(33) Kamaly, N.; Xiao, Z.; Valencia, P. M.; Radovic-Moreno, A. F.; Farokhzad, O. C. *Chem. Soc. Rev.* **2012**, *41*, 2971−3010.
(34) Kent, C. A.; Liu, D.; Meyer, T. J.; Lin, W. *J. Am. Chem. Soc.* **2012**, *134*, 3991−3994.
(35) Lu, G.; Hupp, J. T. *J. Am. Chem. Soc.* **2010**, *132*, 7832−7833.
(36) Lin, W.; Rieter, W. J.; Taylor, K. M. L. *Angew. Chem., Int. Ed.* **2009**, *48*, 650−658.
(37) Oh, M.; Mirkin, C. A. *Angew. Chem., Int. Ed.* **2006**, *45*, 5492−5494.
(38) Lan, A.; Li, K.; Wu, H.; Olson, D. H.; Emge, T. J.; Ki, W.; Hong, M.; Li, J. *Angew. Chem., Int. Ed.* **2009**, *48*, 2334−2338.
(39) Chen, B.; Wang, L.; Xiao, Y.; Fronczek, F. R.; Xue, M.; Cui, Y.; Qian, G. *Angew. Chem., Int. Ed.* **2009**, *48*, 500−503.
(40) Jiang, Y.-Y.; Ren, S.-K.; Ma, J.-P.; Liu, Q.-K.; Dong, Y.-B. *Chem.—Eur. J.* **2009**, *15*, 10742−10746.
(41) Chen, B.; Wang, L.; Zapata, F.; Qian, G.; Lobkovsky, E. B. *J. Am. Chem. Soc.* **2008**, *130*, 6718−6719.
(42) Xie, Z.; Ma, L.; deKrafft, K. E.; Jin, A.; Lin, W. *J. Am. Chem. Soc.* **2010**, *132*, 922−923.
(43) Qi, X.-L.; Lin, R.-B.; Chen, Q.; Lin, J.-B.; Zhang, J.-P.; Chen, X.-M. *Chem. Sci.* **2011**, *2*, 2214−2218.
(44) Qi, X.-L.; Liu, S.-Y.; Lin, R.-B.; Liao, P.-Q.; Ye, J.-W.; Lai, Z.; Guan, Y.; Cheng, X.-N.; Zhang, J.-P.; Chen, X.-M. *Chem. Commun.* **2013**, *49*, 6864−6866.
(45) Takashima, Y.; Martínez, V. M.; Furukawa, S.; Kondo, M.; Shimomura, S.; Uehara, H.; Nakahama, M.; Sugimoto, K.; Kitagawa, S. *Nat. Commun.* **2011**, *2*, 168.
(46) Wanderley, M. M.; Wang, C.; Wu, C.-D.; Lin, W. *J. Am. Chem. Soc.* **2012**, *134*, 9050−9053.
(47) Siegel, R.; Naishadham, D.; Jemal, A. *Ca—Cancer J. Clin.* **2013**, *63*, 11−30.
(48) Choi, K. Y.; Liu, G.; Lee, S.; Chen, X. *Nanoscale* **2012**, *4*, 330−342.
(49) Davis, M. E.; Chen, Z.; Shin, D. M. *Nat. Rev. Drug Discovery* **2008**, *7*, 771−782.
(50) Della Rocca, J.; Liu, D.; Lin, W. *Acc. Chem. Res.* **2011**, *44*, 957−968.
(51) Taylor-Pashow, K. M. L.; Della Rocca, J.; Xie, Z.; Tran, S.; Lin, W. *J. Am. Chem. Soc.* **2009**, *131*, 14261−14263.
(52) Rieter, W. J.; Taylor, K. M. L.; An, H.; Lin, W.; Lin, W. *J. Am. Chem. Soc.* **2006**, *128*, 9024−9025.
(53) Taylor, K. M. L.; Jin, A.; Lin, W. *Angew. Chem., Int. Ed.* **2008**, *47*, 7722−7725.
(54) Taylor, K. M. L.; Rieter, W. J.; Lin, W. *J. Am. Chem. Soc.* **2008**, *130*, 14358−14359.
(55) deKrafft, K. E.; Xie, Z.; Cao, G.; Tran, S.; Ma, L.; Zhou, O. Z.; Lin, W. *Angew. Chem., Int. Ed.* **2009**, *48*, 9901−9904.
(56) Horcajada, P.; Serre, C.; Vallet-Regí, M.; Sebban, M.; Taulelle, F.; Férey, G. *Angew. Chem., Int. Ed.* **2006**, *45*, 5974−5978.
(57) Horcajada, P.; Serre, C.; Maurin, G.; Ramsahye, N. A.; Balas, F.; Vallet-Regí, M. a.; Sebban, M.; Taulelle, F.; Férey, G. r. *J. Am. Chem. Soc.* **2008**, *130*, 6774−6780.
(58) An, J.; Geib, S. J.; Rosi, N. L. *J. Am. Chem. Soc.* **2009**, *131*, 8376−8377.
(59) Zou, H.; Wu, S.; Shen, J. *Chem. Rev.* **2008**, *108*, 3893−3957.
(60) Lu, Y.; Yin, Y.; Mayers, B. T.; Xia, Y. *Nano Lett.* **2002**, *2*, 183−186.
(61) Rieter, W. J.; Taylor, K. M. L.; Lin, W. *J. Am. Chem. Soc.* **2007**, *129*, 9852−9853.
(62) Zhao, D.; Tan, S.; Yuan, D.; Lu, W.; Rezenom, Y. H.; Jiang, H.; Wang, L.-Q.; Zhou, H.-C. *Adv. Mater.* **2011**, *23*, 90−93.
(63) Liu, D.; Kramer, S. A.; Huxford-Phillips, R. C.; Wang, S.; Della Rocca, J.; Lin, W. *Chem. Commun.* **2012**, *48*, 2668−2670.
(64) Baati, T.; Njim, L.; Neffati, F.; Kerkeni, A.; Bouttemi, M.; Gref, R.; Najjar, M. F.; Zakhama, A.; Couvreur, P.; Serre, C.; Horcajada, P. *Chem. Sci.* **2013**, *4*, 1597−1607.
(65) deKrafft, K. E.; Boyle, W. S.; Burk, L. M.; Zhou, O. Z.; Lin, W. *J. Mater. Chem.* **2012**, *22*, 18139−18144.
(66) Liu, D.; Huxford, R. C.; Lin, W. *Angew. Chem., Int. Ed.* **2011**, *50*, 3696−3700.
(67) Nishiyabu, R.; Hashimoto, N.; Cho, T.; Watanabe, K.; Yasunaga, T.; Endo, A.; Kaneko, K.; Niidome, T.; Murata, M.; Adachi, C.; Katayama, Y.; Hashizume, M.; Kimizuka, N. *J. Am. Chem. Soc.* **2009**, *131*, 2151−2158.